Ionization and ionic fragmentation of tetrahydrofuran molecules by electron collisions

Marcin Dampc, Ewelina Szymańska, Brygida Mielewska, Mariusz Zubek

Ionization and ionic fragmentation of tetrahydrofuran molecules by electron collisions

Marcin Dampc, Ewelina Szymańska*, Brygida Mielewska and Mariusz Zubek

Department of Physics of Electronic Phenomena,

Gdańsk University of Technology, 80-233 Gdańsk, Poland

Abstract

Electron impact ionization and ionic fragmentation of tetrahydrofuran molecules in the gas phase was studied in the energy range from ionization threshold up to 150 eV using technique of mass spectrometry. The cation mass spectra, ionization and ionic fragmentation efficiencies were measured over this energy range. Well resolved mass peaks were detected in the mass range 10-72 amu and assigned to corresponding ionic molecular fragments. The most abundant cation in the mass spectra is at 42 amu. Appearance energies of selected ionic fragments were also determined. Possible ionic fragmentation processes are discussed.

*Present address: Department of Physics and Astronomy, The Open University, Milton Keynes, UK

PACS: 34.80 Gs

1. Introduction

The interaction of high energy radiation, electrons, ions and radicals with biomolecules, in particular with the DNA fragments, nucleic purine and pyrimidine bases, phosphate units and deoxyribose sugar, has been extensively studied to uncover effects of primary and secondary particles in radiation damage of living cells and other biological systems[1-6]. The secondary electrons, which are produced in large quantities by the primary ionizing particles in the biological material, may cause single- and double strand breaks in the polynucleotides of DNA through site selective cleavage of the molecular bonds. The molecular bonds in the repeated sugar-phosphate backbones and also in the four fundamental nucleic bases attached to the backbone by covalent bonds are ruptured efficiently through processes of dissociative electron attachment, neutral fragments dissociation and dissociative ionization. For example, the gas phase studies of dissociative electron attachment to purine (adenine and guanine) and pyrimidine (thymine and cytosine) bases showed that they undergo electron-induced fragmentation in the subionization energy range (<10 eV) where the density of the secondary electrons is high [7,8]. These secondary electrons produced by the primary radiation, which in the pre-thermalization period possess energies greater than 10 eV but below 100 eV, will efficiently induce dissociative ionization of the targets, because of the high associated value of collision cross section for low electron impact energies. In order to determine the most sensitive part of the DNA or RNA molecular chains to electron-induced bond rupture thorough studies of reactions to electrons of their building structures and combinations of these structures, e. g. nucleic bases and phosphate-sugar groups were investigated [9-11]. These recent studies demonstrated that it is the deoxyribose (2-deoxy-D-ribose), which is most likely damaged in producing strand breaks in DNA or RNA [12,13].

Deoxyribose, $C_5H_{10}O_4$ (D) is a constituent of the sugar-phosphate backbone of the DNA and RNA polynucleotide chains and bonds with the nucleic bases. In the chain, it is in the

furanose form of a five-membered carbon, oxygen ring with the CH_2 group attached to C(2) atom and providing bonds to phosphate group and nuclei bases at C(3) and C(5), respectively (figure 1a). However, in the gas phase D is predominantly in the pyranose form of six-membered ring and in order to study specifically the strength of the furanose ring under electron interactions several analogues, α-tetrahydrofurfuryl alcohol (THFA), 3-hydroxytetrahydrofuran (3HTHF) and tetrahydrofuran (THF) molecules have been used as corresponding targets [14]. The THF, C_4H_8O molecule (figure 1b) is often considered as the simplest analogue to deoxyribose. In the two other analogues, as compared to THF, the hydrogen atoms at position (2) and (3) are replaced by CH_2OH and OH radicals, respectively. Thus, THF molecules became recently a frequent subject of experimental investigations of electron interactions, elastic scattering [15-17], vibrational excitation [17-19] and dissociative electron attachment [20,21] in the gas phase. Vibrational excitation [18] and H^- desorption [22] in the electron interaction with deposited thin film layers were also studied.

In this paper we present investigations of the electron-induced ionization and ionic fragmentation of the THF molecules in the gas phase, in the energy range from the ionization threshold up to 150 eV. The cation mass spectra at selected electron energies and the cation fragmentation efficiencies curves were measured using technique of mass spectrometry. A significant amount of work were also put into determination of appearance energies (AE) of ionic fragments. Earlier, electron impact mass spectra of the THF molecule were measured by Gallegos and Kiser [23] at 70 eV and by Collin and Conde-Caprace [24] in the 10-50 eV range (see this reference for other earlier works). These authors also determined the AE of the most abundant ionic fragments and analyzed possible paths of the THF fragmentation from their thermochemical calculations. The results of Ref.s [23, 24] are displayed in the NIST database [25]. Duffield *et al.* [26] obtained mass spectra of five-membered

heterocycles including the THF and studied fragmentation modes of the THF by deuterium labeling method. Very recently, Fuss *et al.* [27] measured the time-of-flight ionic mass spectra of the THF over extended energy range 50-5000 eV, however with a limited mass resolution. These authors also carried out the total ion collection measurements to determine total ionization cross section of the THF. The total ionization cross section of the THF was calculated by Możejko and Sanche [28] in the binary-encounter-Bethe approach. Photon induced ionic fragmentation of the THF in the gas phase was studied very recently by Mayer *et al* [29] using tunable synchrotron radiation. The AEs obtained for the observed ionic molecular fragments are lower (by 1-3 eV) than those obtained by electron impact in Ref.s [23, 24]. Applied threshold photoelectron photoion coincidence technique allowed breakdown curves for the detected ions to be measured in the energy range up to 35eV.

The measurements of this work were performed using a quadrupole mass spectrometer for the ion mass analysis and the mass spectra were recorded at selected electron energies. A number of well resolved mass peaks were detected in the mass range 10-72 amu and were assigned to corresponding ionic fragments. These spectra resolved some inconsistencies between earlier works (NIST data) and mass spectra published very recently [27], as will be described later. The AE of the identified cations were determined from the ion efficiency curves measured over the threshold regions by applying a fitting procedure. The cation efficiency curves measured in the 5-150 eV energy range were normalized with reference to mass spectra to determine contributions of the individual cations to the total ionization cross section. Motivation of the present work is to provide data of the partial and total ionization efficiencies which may serve as the input parameters in modeling radiation-induced damage in the biomolecular systems.

2. Experimental

The measurements of the cation mass spectra at a fixed electron energy and the ionic fragment efficiencies of the THF as a function of electron energy were carried out using quadrupole mass spectrometer EPIC 300 (Hiden Analytical Ltd.). The spectrometer incorporates an electron ionizer, an ion extractor and focusing lens electrodes, a quadrupole mass filter and a secondary electron multiplier for ion detection. The THF vapour was delivered into the system by a narrow stainless steel capillary positioned 5 mm from the ionization cage. The spectrometer was mounted in a vacuum chamber evacuated by a 60 ls^{-1} turbomolecular pumping unit to a base pressure of 2×10^{-7} mbar which increased to the operating pressure of 1×10^{-6} mbar when introducing the target THF vapour. During the measurements electron incident current in the ionizer was 2-10 μA. Linear dependences between the operating pressure, the incident electron current and the detected ion signal were maintained. As the THF cations formed in the ionic fragmentation may carry initial translation energy, it was also ensured that the measured mass spectra are independent of the spectrometer tuning for ion kinetic energies in the range 0-3 eV. The estimated transit time from the ionization region to the detector of 50 amu ions, at 3 eV ion kinetic energy was 50 μs. The ionic fragment efficiency curves obtained in the 5-150 eV range were corrected for the energy variation of the electron incident beam. Here, argon Ar^+ ions yields were recorded in a mixture with the THF and compared with argon ionization cross section [30] to deduce the correction factor. The background signal was measured at the base pressure of 2×10^{-7} mbar and subsequently subtracted from the original spectra.

The mass dependence of transmission of the quadrupole spectrometer was tested by measuring the mass spectra of carbon dioxide and comparing these results with the literature cross sections for CO_2 fragment ions [31]. It was found that the transmission is constant in the mass region from the 28 amu (CO^+/CO_2) to 44 amu ($CO_2{}^+/CO_2$), which is the region in which the majority of the THF cation fragments appear. In determination of the relative cation efficiencies of the THF it was assumed that the ion transmission does not vary appreciably for masses outside

of this region and that the transmission for masses of 15, 71 and 72 amu is equal to that of the 28-44 amu region. This assumption may introduce increased uncertainty in the relative intensities of the above ions. However, it was found that when varying their contributions into the total ion efficiency curve it had small effect on the overall shape of the curve. The electron energy was calibrated against known AE of Ar^+ (15.75 eV) to within ± 0.15 eV. The measurements of Ar^+ yield in the region above AE enabled a value of 600 meV for the energy spread of the incident electron beam to be deduced.

The anhydrous liquid THF was placed in a stainless steel container attached to a gas line. which was maintained at the room temperature. Heating of the sample was not required as the THF has sufficiently high vapour pressure at this temperature. It was degassed several times under low pressure to remove contaminating gases, nitrogen, oxygen and water vapour, before introducing into the spectrometer by a leak valve, which was heated to avoid THF condensation. The THF mass spectra measured simultaneously showed decreasing intensities of these contaminations to a level much lower than that of the THF ions. THF was purchased from Sigma-Aldrich Chemie with a stated purity of 99.9 %.

The AEs of the observed ionic molecular fragments were determined from the ion efficiency yields measured in an energy region of about 5 eV positioned symmetrically against the expected AE threshold. To determine accurate values of AE the efficiency curves were fitted with an exponential near-threshold cross section function

$$\begin{aligned} \sigma(E) &= 0 , \quad E \leq E_A \\ \sigma(E) &= c(E - E_A)^n, \quad E > E_A \end{aligned} \qquad (1)$$

which was convoluted with the Gaussian electron energy spread. The parameters involved in the fitting are, E_A the appearance energy, c the scaling factor and n the exponential constant. The above procedure based on an exponential expression (1) was introduced by Märk [32] and further developed by Matt *et al* [33] and used extensively thereafter [14]. The uncertainties of the

obtained AEs which take into account the uncertainty in energy calibration and the standard deviations of the mean values of AEs are given in table 2 together with the values of AEs.

3. Results and discussion

Electron collisions with THF molecules in the gas phase lead to ionization into the parent $C_4H_8O^+$ cation and formation of a number of cationic fragments. The mass spectrum of THF cations measured at an incident electron energy of 140 eV is shown in figure 2 together with tentative assignments of the observed mass peaks. Spectra with nearly identical peak intensities were also obtained at 70 eV. The relative abundances of the cations seen in the main spectrum of figure 2 are listed in table 1 in percentage ratio to the most intense mass of 42 amu. The AEs, which were determined for the individual ionic fragments, are presented in table 2 as mean values derived from several determinations and are compared with results of other works [23, 24, 29]. Figure 3 shows ionization efficiency curves obtained in the threshold regions for masses of 71, 42, 41, 29 amu and illustrates the high quality of the fitting obtained in the determination of the ionic AEs from the indicated exponential functions.

3.1. Mass spectrum of THF

The cation peaks in the mass spectrum of THF appear in two distinct groups occurring in the mass ranges 26-31 and 37-45 amu, respectively. Two further intense peaks are seen at masses 71 and 72 amu. Low intensity peaks are detected at mass 15 amu and also at 1 and 2 amu (not shown in figure 2). The most abundant cation is observed at mass 42 amu and the second most abundant cation at mass 41 amu, both having intensities higher than that of the parent $C_4H_8O^+$ ion of mass 72 amu. The inset of figure 2 shows the mass spectrum in the range 46-62 amu, which covers the region of low abundance cations with relative intensities below 0.6 %. The 54, 55 and 57 amu peaks may correspond to impurities, because their intensities decreased with time of the measurements. The spectrum of figure 2 is in very good agreement with the NIST database [25]. The time-of-flight spectrum of Fuss *et al* [27] measured at 1000 eV shows unresolved groups of

cation peaks near 29, 40 and 72 amu, consistent with our high resolution mass spectrum of figure 2. It also shows a wider mass peak of high intensity around 52 amu that is not confirmed by our results (see inset of figure 2), and neither by the NIST data. This disagreement cannot be caused by the difference in electron energies of both measurements, as the 52 amu peak in the Fuss *et al* data appears also and dominates at lower energies. For example, at 150 eV it gives a 42 % contribution to the total ionization cross section. The above disagreement between both mass spectra could be rationalized if the 52 amu ions have a relatively short lifetime and decay in-flight before being detected in our mass spectrometer. However, our estimations of the ion transit times based on the experimental details in both measurements show that the times are comparable (30-50 μs).

Some conclusions may be drawn from comparison of the THF mass spectrum of the present work and that of the other analogues, THFA and 3HTHF [14] with the cation mass spectrum of D [12]. The mass spectra of all four molecules display groups of cations in the 26-32 and 39-45 amu regions. The 15-20 amu cations in THFA and 3HTHF have lower relative intensities than that in D while in THF that group is reduced to a single peak at 15 amu. The group of 55-61 amu cations are seen in the D and 3HTHF spectra but not in that of THFA and THF. None of the cation groups around 70 amu in the mass spectra of the analogues resemble that of the D spectrum, which contains more fragments than the analogue molecules. The parent ion has the highest abundance in the case of THF (32%) and it is reduced to 10.8 % in 3HTHF [41]. In THFA the parent ion abundance is lower than 1.5 % and resembles the situation for D. It may be concluded that bonding of several functional groups or a single group but of higher mass to the furanose ring lowers the strength of the cation ring and fragmentation via ring rapture becomes more favourable. It is also of note that photofragmentation of D in the gas phase [13] produces similar groups of cations to that obtained in electron impact ionization, although with different relative abundances of the individual groups.

3.2 Fragmentation processes

The parent $C_4H_8O^+$ ion is formed by ionization from the highest occupied non-bonding oxygen atom lone-pair 9b/12a´ (C_2/C_s THF conformations) orbital. Its abundance is about three times lower than that of the most intense ion peak at 42 amu. The AE obtained for $C_4H_8O^+$ ion is 9.55 ± 0.15 eV and this value is consistent with the previous electron impact [23,24] and photoionization [29, 34, 35] measurements as is shown in Table 2. For comparison, the AE of the parent ion of D is 10.51 ± 0.11 [12]. It is about 1 eV higher than that of THF. The $C_4H_7O^+$ cation (of mass 71 amu) involves electron detachment with simultaneous cleavage of one of the C-H bonds. The ionization takes place from the 9b/12a´ orbital because the $C_4H_7O^+$ AE of 10.20 ± 0.25 eV (figure 3) is lower than the adiabatic ionization energy (10.7 eV) of the next occupied 11a/11a´ orbital [34]. The deuterium labeling method [29] established that 70% of the ions correspond to loss of an α-H atom and the rest to loss of an β-H atom by the THF molecule. Standard ab initio molecular orbital calculations [32] eliminated the possibility that the THF ion dissociates via a ring-opening reaction leading to the distonic $\bullet CH_2CH_2CH_2OCH_2^+$ isomer.

The most abundant ion (mass 42 amu) is identified as the cyclopropane $C_3H_6^+$ ion radical from measurements in deuterium THF derivative [26] and estimations of heat of formation of $C_3H_6^+$ [24]. The neutral fragment with mass 30 amu is the formaldehyde, CH_2O molecule, however formation of CO and H_2 cannot be excluded. This suggests the following reactions

$$C_4H_8O^+ \rightarrow C_3H_6^+ + CH_2O \quad \text{and} \quad C_4H_8O^+ \rightarrow C_3H_6^+ + CO + H_2. \qquad (2)$$

In both cases it requires scission of the C(5)-O(1) and C(2)-C(3) bonds within the ring (see figure 1a). The AE obtained for the $C_3H_6^+$ cation is equal to 11.4 ± 0.25eV (figure 3) and agrees well with the value of Ref. [24]. It coincides with the vertical ionization potential of the 11a/11a´ orbital (11.37 eV [35]), while the AE of $C_3H_6^+$ of 10.65 ± 0.2 eV obtained in photoionization measurements [29] agrees well with the adiabatic ionization energy of the 11a/11a´ orbital. This may suggest, in both electron impact and photoionization, a reaction channel where an electron is

removed from the 11a/11a´ ($n_{O||}$,σ_{CC}) orbital. This would weaken the respective C-O and C-C bonds and initiate dissociation of the $C_4H_8O^+$ ion.

The second most abundant cation (mass 41 amu) corresponds to $C_3H_5^+$ in both conformations of linear and cyclopropenyl ions [24,26]. The neutral products are the methoxy, CH_3O radical or the formaldehyde molecule and an H atom [24] giving the two following reactions

$$C_4H_8O^+ \rightarrow C_3H_5^+ + \bullet CH_3O \quad \text{and} \quad C_4H_8O^+ \rightarrow C_3H_5^+ + CH_2O + H. \qquad (3)$$

The first reaction requires rearrangement of the H atoms in the THF ion [24]. The present AE is lower than that from two previous electron impact measurements [23, 24] and is just above the value obtained in the photoionization studies [29] (see Table 2). The efficiency curve in the threshold region was fitted with an exponential function with *n*=2.2 (figure 3) which is higher than for the case of Ar^+, where *n*=1. Higher values of *n* correspond to a slower increase of the ionic cross section in the threshold region, which may result from excitation of the internal energy levels (vibrational and electronic) of the cation. The $C_3H_5^+$ ionic fragment is again formed by breaking of the C-C and C-O bonds in the furanose ring.

The most obvious reactions producing cations of the masses 43 and 44 amu are

$$C_4H_8O^+ \rightarrow C_2H_3O^+ + C_2H_4 + H \quad \text{and} \quad C_4H_8O^+ \rightarrow C_2H_4O^+ + C_2H_4, \qquad (4)$$

respectively, both involving the release of a neutral ethylene molecule. The AE of the $C_2H_3O^+$ cation, 10.90 ± 0.25 eV is equal to a value obtained in the photoionization investigation [26] and is lower than the earlier electron impact results [23, 24]. The value of *n*=2.2 obtained in the efficiency curve fitting again points at a possible excitation of the internal energy levels of the cation. The 39 and 40 amu peaks in the mass spectrum correspond to the $C_3H_3^+$ and $C_3H_4^+$ cations, respectively formed by cleavage of the C-C and C-O bonds and further detachment of the H atoms.

The abundances of cations in the 26-31 amu region are lower than 20% (Table 1). The peaks at 26, 27 and 28 amu can be unambiguously assigned to acetylene, $C_2H_2^+$, deprotonated ethylene,

$C_2H_3^+$ and ethylene, $C_2H_4^+$ cations. The AE of the $C_2H_2^+$ coincides with that of $C_3H_6^+$ implying probable decay of the $C_3H_6^+$ cation by CH_4 release. The $C_2H_3^+$ fragment has the highest abundance of the above three cations and it may be formed in the reaction

$$C_4H_8O^+ \rightarrow C_2H_3^+ + CH_2O + CH_3 . \quad (5)$$

The 29 and 31 amu peaks are assigned to the CHO^+ and CH_3O^+ cations, respectively. Here, a similarity with the tetrahydrothiophene, C_4H_8S molecule was exploited. For this molecule, the deuterium labeling method [26] showed the origins of the corresponding CHS^+ and CH_3S^+ cations. The 15 amu peak is due to the methyl CH_3^+ cation. The above low-mass cations involve multiple bonds rearrangement and hydrogen atoms transfer along the ring in the processes of fragmentation. The present AEs of the ionic fragments in the 15-40 amu range are lower than the earlier electron impact values [23] and are closer to the corresponding photoionization results [26].

3.3 Partial and total ionic efficiency curves

The ionic efficiency curves of the THF fragments recorded in the mass spectrum of figure 2 were measured from 5 to 150 eV. These curves were normalized to each other according to abundances at 140 eV given in Table 1. Figure 4 displays examples of the curves obtained for cations of 72, 44, 42, 26 and 15 amu, respectively. Sum of the partial efficiency curves of the individual ionic fragments represents the relative total ionization cross section. Figure 5 compares the total ionization cross section with the results of binary-encounter-Bethe calculations [28]. This approach predicts the total ionization cross section as the sum of the ionization cross sections for removing one electron from each of the molecular orbitals that contribute to ionization [36]. The ionization cross section is given by a simple analytic expression, as a function of incident electron energy, which does not include details of ionization routes. For comparison both results are normalized to unity at their maxima. There is a general agreement between the experimental and

calculated cross sections, although the experimental curve rises faster above threshold and displays a maximum at a lower electron energy of 58.5 eV.

4. Conclusions

This work reports measurements of the cation mass spectra, ionization and ionic fragmentation efficiency curves of the THF molecules in the electron energy range 5-150 eV using mass spectrometry technique. A number of well resolved mass peaks were detected in the mass range 10-72 amu and assigned to the corresponding ionic molecular fragments. The mass spectra are in good agreement with the NIST data. The present spectra resolved some inconsistencies between NIST data and the mass spectra published very recently [27]. The AEs of the identified cations were also determined. The present values of AEs do not confirm some of the early electron impact measurements. The cation efficiency curves measured over the 5-150 eV range were normalized to each other with a reference to the mass spectra to determine their contributions to the total ionization cross section. The sum of the cation efficiency curves, which gives the relative total ionization cross section is compared with the binary-encounter-Bethe calculations [28]. There is a general agreement between the experimental and calculated cross sections, although the experimental curve rises faster above threshold and displays a maximum at a lower electron energy. These differences may further indicate that the binary-encounter-Bethe method can not give account of ionic fragmentation in ionization.

The cation mass spectrum of the THF is compared with that of D. It is concluded that in the case of ionization and ionic fragmentation THF has some limits to be considered as an equivalent analogue of D. This conclusion corroborates that of the dissociative electron attachment studies which “demonstrated that THF cannot be used as a surrogate to model deoxyribose in DNA with respect to the attack of electrons at subexcitation energies (<3 eV)” [21].

Acknowledgements

This work was carried out within COST Action CM0601 “Electron Controlled Chemical Lithography”. It was supported by the Polish Ministry for Science and Higher Education under contract 553/N-COST/2009/0 .

References

[1] Sanche L 2005 Eur. Phys. J. D **35** 367

[2] Bernhardt Ph, Friedland W, Jacob P and Paretzke H G 2003 I. J. Mass Spectrom. **223-224** 579

[3] Coupier B *et al.*2002 Eur. Phys. J. D **20** 459

[4] Bari S *et al.* 2008 J. Chem. Phys. **128** 074306

[5] Martin S, Brédy R, Allouche A R, Bernard J, Salmoun A, Li B and Chen L 2008 Phys. Rev. A **77** 062513

[6] Surdutovich E, Obolensky O I, Scifoni E, Pschenichnov I, Mishustin I, Solov’yov A V and Greiner W 2009 Eur. Phys. J. **51** 63

[7] Denifl S Ptasińska S, Probst M, Hrušák J J, Scheier P and Märk T D 2004 J. Phys Chem. A **108** 6562

[8] Huber D, Beikircher M, Denifl S, Zappa F, Matejčik S, Bacher A, Grill V, Märk T D and Scheier P 2006 J. Chem. Phys. **125** 084304

[9] Zheng Y, Cloutier P, Hunting D J, Wagner J R and Sanche L 2006 **124** 64710

[10] Solomun T, Seitz H and Sturm H 2009 J. Phys. Chem. B **113** 11557

[11] Li Z, Zheng Y, Cloutier P, Sanche L and Wagner J R 2008 **130** 5612

[12] Ptasińska S, Denifl S, Scheier P and Märk T D 2004 J. Chem. Phys. **120** 8505

[13] Vall-Ilosera G, Huels M A, Coreno M, Kivimäki A, Jakubowska K, Stankiewicz M and Rachlew E 2008 ChemPhysChem **9** 1020

[14] Milosavljević A R, Kočišek J, Papp P, Kubala D, Marinković B P, Mach P, Urban J and

Matejčík Š 2010 J. Chem. Phys. **132** 10430

[15] Colyer C J, Vizcaino V, Sullivan J P, Brunger M J and Buckman S J 2007 New J. Phys. **9** 41

[16] Dampc M, Milosavljević A R, Linert I, Marinković B P and Zubek M 2007 Phys. Rev. A **75** 042710

[17] Allan M 2007 J. Phys B: At. Mol. Opt. Phys. **40** 3531

[18] Lepage M, Letarte S, Michaud M, Motte-Tollet F, Hubin-Franskin M.-J., Roy D and L.Sanche 1998 J. Chem. Phys. **109** 5980

[19] Dampc M, Linert I, Milosavljević A R and Zubek M 2007 Chem. Phys. Lett. **443** 17

[20] Ibănescu B C, May O and Allan M 2008 Phys. Chem. Chem. Phys. **10** 1507

[21] Sulzer P, Ptasińska S, Zappa F, Mielewska B, Milosavljević A R, Scheier P and Märk T D 2006 J. Chem. Phys. **125** 044304

[22] Antic D, Parenteau L and Sanche L 2000 J. Phys. Chem. B **104** 4711

[23] Gallegos E J and Kiser R W 1962 J. Phys. Chem **66** 136

[24] Collin J E and Conde-Caprace G 1968 I. J. Mass Spectrom. Ion Phys. **1** 213

[25] NIST chemistry web book, http://webbook.nist.gov

[26] Duffield A M, Budzikiewicz H and Djerassi C 1965 J. Am. Chem. Soc. **87** 2920

[27] Fuss M, Muñoz A, Oller J C, Blanco F, Almeida D, Limão-Vieira P, Do T P D, Brunger M J and García G 2009 Phys. Rev. A **80** 052709

[28] Możejko P and Sanche L 2005 Rad. Phys. Chem. **73** 77

[29] Mayer P M, Guest M F, Cooper L, Shpinkova L G, Rennie E E, Holland D M P and Shaw D A 2009 J. Phys. Chem. A **113** 10923

[30] Rejoub R, Lindsay B G and Stebbings R F 2002 Phys. Rev. A **65** 042713

[31] King S J and Price S D 2008 I. J. Mass Spectrom. **272** 154

[32] Märk T D 1975 J. Chem. Phys. **63** 3731

[33] Matt S, Echt O, Wörgötter R, Grill V, Scheier P, Lifshitz C and Märk T D 1997 Chem.

Phys. Lett. **264** 149

[34] Dampc M, Mielewska B, Siggel-King M R F, King G C and Zubek M 2009 Chem. Phys. **359** 77

[35] Wang J, Yang B, Cool T A, Hansen N and Kasper T 2008 I. J. Mass Spectrom. **269** 210

[36] Hwang W, Kim Y-K and Rudd M E 1996 J. Chem. Phys. **104** 2956

Figure captions

Figure 1.
Schematic diagrams of, (a) fragment of the DNA molecule containing sugar, cytosine and phosphate groups, (b) tetrahydrofuran, C_4H_8O molecule. Labeling of atoms is shown for the tetrahydrofuran molecule. Color code: the carbon atom is gray, oxygen atom red, hydrogen atom light gray, phosphorus atom purple and nitrogen atom blue.

Figure 2.
The mass spectrum of cations of tetrahydrofuran molecules recorded at an electron energy of 140eV. The inset shows in detail the mass range from 48 to 60 amu.

Figure 3.
The ionic efficiency curves for cations of m = 71, 42, 41, 29 amu of tetrahydrofuran molecules measured in the near-threshold regions. The solid lines show curves of the indicated exponential functions fitted to the experimental data. The appearence energies are indicated by arrows.

Figure 4.
The ionic efficiency curves for cations of m = 72, 44, 42, 26, 15 amu of tetrahydrofuran molecules measured in the electron energy range 5-150eV.

Figure 5.
The total ionization cross sections of tetrahydrofuran molecules obtained in the electron energy range 5-150eV in the present measurements and in the binary-encounter-Bethe calculations of Możejko and Sanche [28]. For comparison both curves are normalized to unity at their maxima.

Table 1.

Abundances and assignments of cations of tetrahydrofuran molecules measured at an electron energy of 140 eV.

m (amu)	Cation assignment	Relative abundance
72	$C_4H_8O^+$	32%
71	$C_4H_7O^+$	30%
44	$C_2H_4O^+$	4%
43	$C_2H_3O^+$	19%
42	$C_3H_6^+$	100%
41	$C_3H_5^+$	40%
40	$C_3H_4^+$	8%
39	$C_3H_3^+$	10%
31	CH_3O^+	3%
29	CHO^+	9%
28	$C_2H_4^+$	5%
27	$C_2H_3^+$	17%
26	$C_2H_2^+$	3%
15	CH_3^+	4%

Table 2.

Appearance energies (in eV) of cations of tetrahydrofuran molecules obtained in the present work, compared with electron impact (EI) and photoionization (PI) measurements.

m (amu)	Present work	Meyer et al PI	Gallegos and Kiser EI	Collin and Conde-Caprace EI
72	9.55 ± 0.15	9.445 ± 0.010	9.45 ± 0.15	9.55
71	10.20 ± 0.25	<10.0 ± 0.1	11.1 ± 0.2	10.44
45		12.15 ± 0.10		
44		11.0 ± 0.1		12.27
43	10.90 ± 0.25	10.9 ± 0.2	12.8 ± 0.2	11.87
42	11.40 ± 0.25	10.65 ± 0.20	12.7 ± 0.2	11.54
41	12.9 ± 0.2	12.7 ± 0.2	15.5 ± 0.3	13.72
40	13.50 ± 0.25	12.9 ± 0.2	15.2 ± 0.3	
39	15.6 ± 0.2	14.9 ± 0.2	18.7 ± 0.6	
38		23.5 ± 0.2		
37		25 ± 1		
31	12.0 ± 0.2	11.85 ± 0.10		
29	11.65 ± 0.20	12.5 ± 0.2	15.8 ± 0.2	
28	13.95 ± 0.25	12.5 ± 0.2		
27	13.30 ± 0.25	13.3 ± 0.1	16.1 ± 0.3	
26	11.40 ± 0.25	14.9 ± 0.2	17.3 ± 0.3	
16		15.6 ± 0.1		
15	14.0 ± 0.5	16.0 ± 0.3		
14		19.5 ± 0.5		

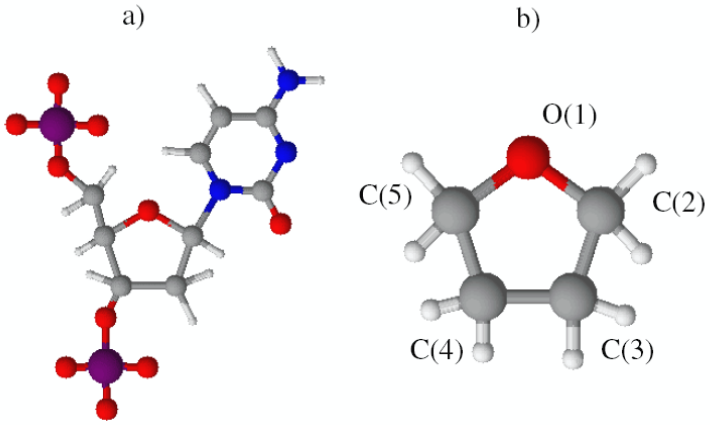
a)
b)
O(1)
C(5)
C(2)
C(4)
C(3)

Fig.1

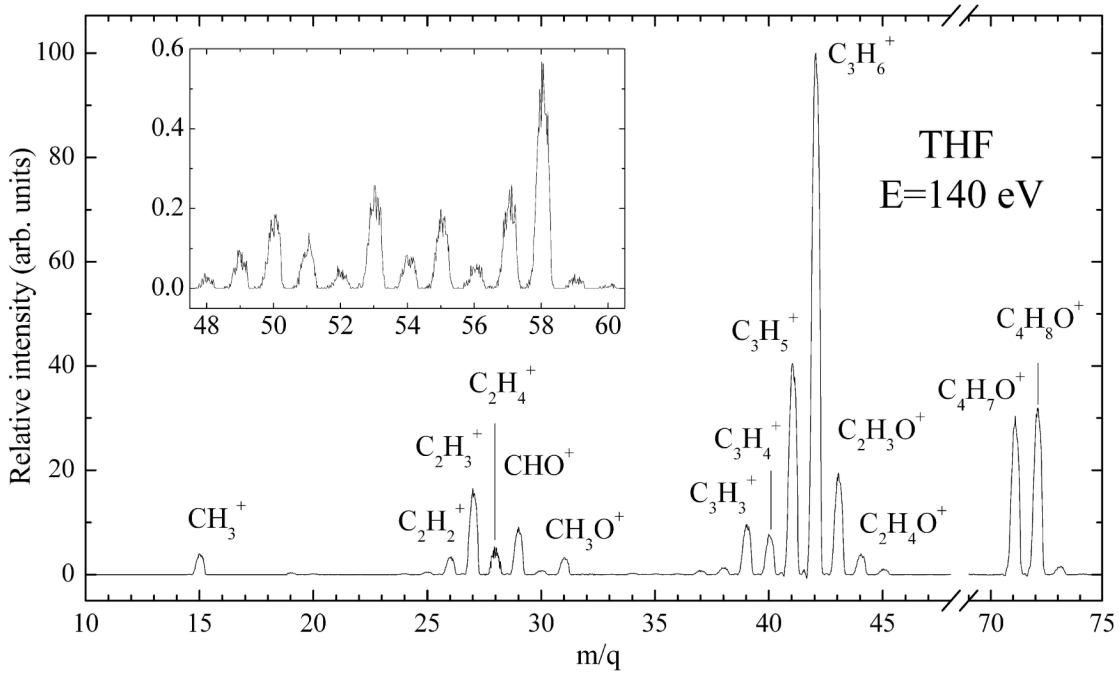
THF
E=140 eV
Relative intensity (arb. units)
m/q
CH3+
C2H2+
C2H3+
CHO+
C2H4+
CH3O+
C3H3+
C3H4+
C3H5+
C3H6+
C2H3O+
C2H4O+
C4H7O+
C4H8O+

Fig. 2

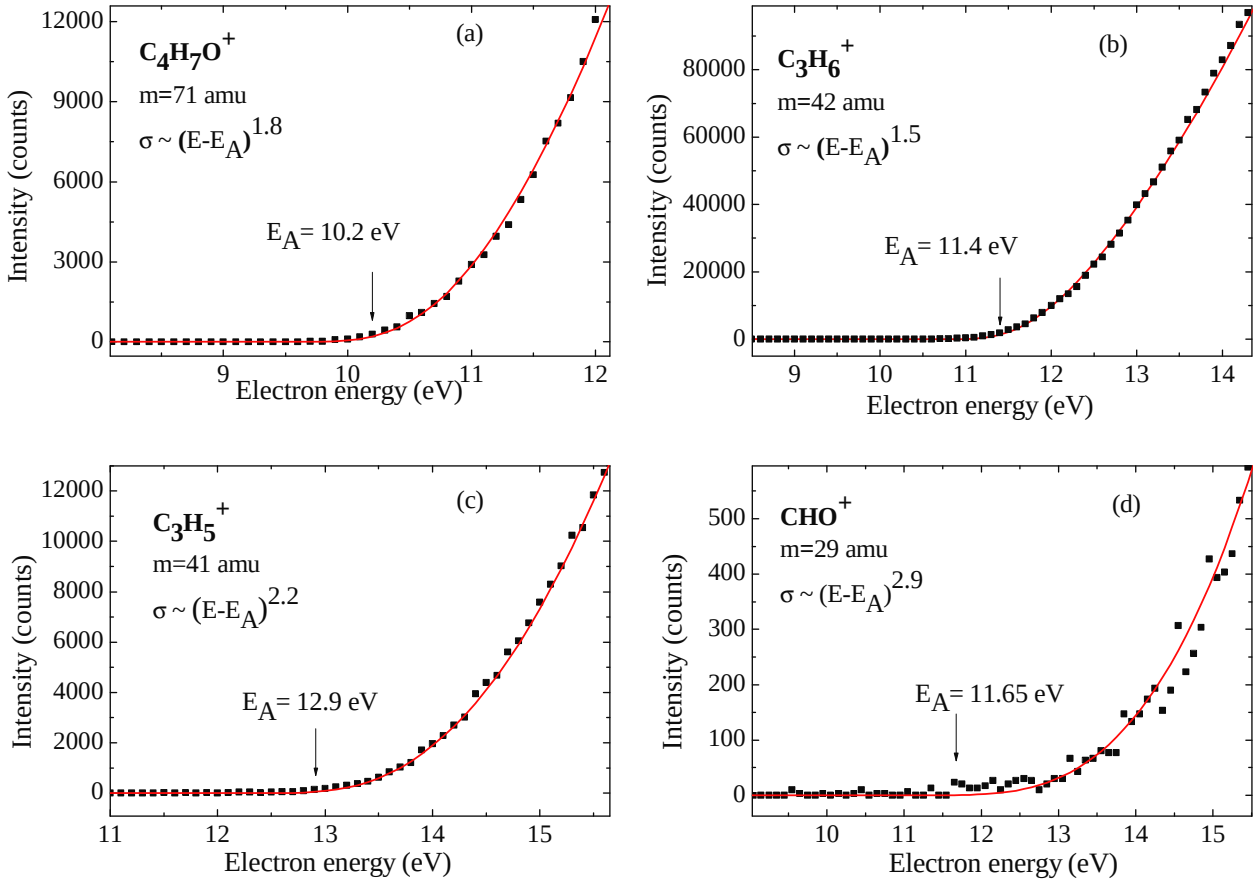
(a)
$C_4H_7O^+$
m=71 amu
σ ~ (E-E$_A$)$^{1.8}$
E$_A$= 10.2 eV
Intensity (counts)
Electron energy (eV)
(b)
$C_3H_6^+$
m=42 amu
σ ~ (E-E$_A$)$^{1.5}$
E$_A$= 11.4 eV
Intensity (counts)
Electron energy (eV)
(c)
$C_3H_5^+$
m=41 amu
σ ~ (E-E$_A$)$^{2.2}$
E$_A$= 12.9 eV
Intensity (counts)
Electron energy (eV)
(d)
CHO^+
m=29 amu
σ ~ (E-E$_A$)$^{2.9}$
E$_A$= 11.65 eV
Intensity (counts)
Electron energy (eV)

Fig. 3

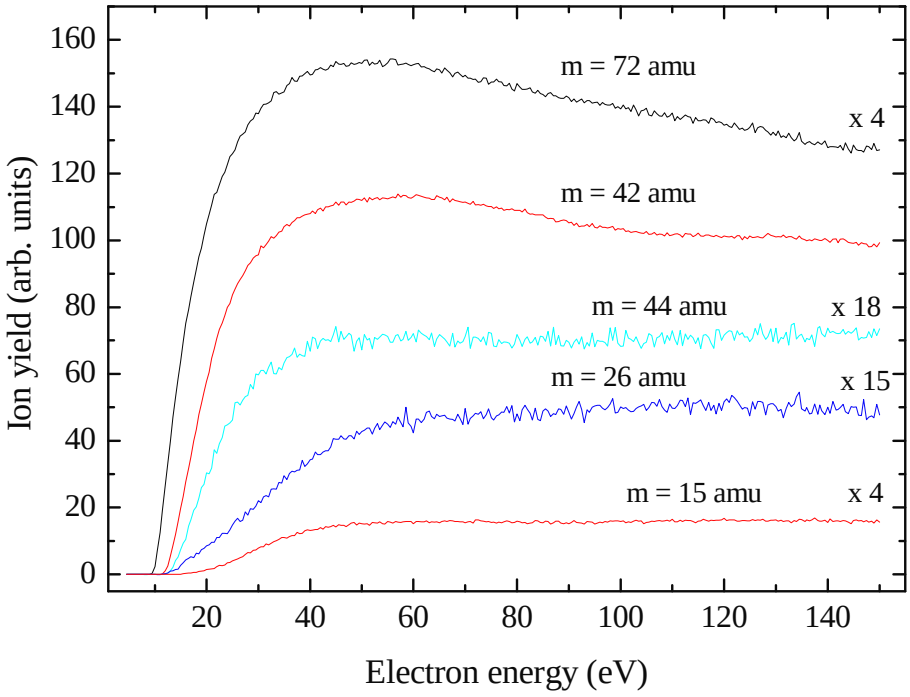
Ion yield (arb. units)
Electron energy (eV)
m = 72 amu
x 4
m = 42 amu
m = 44 amu
x 18
m = 26 amu
x 15
m = 15 amu
x 4

Fig. 4

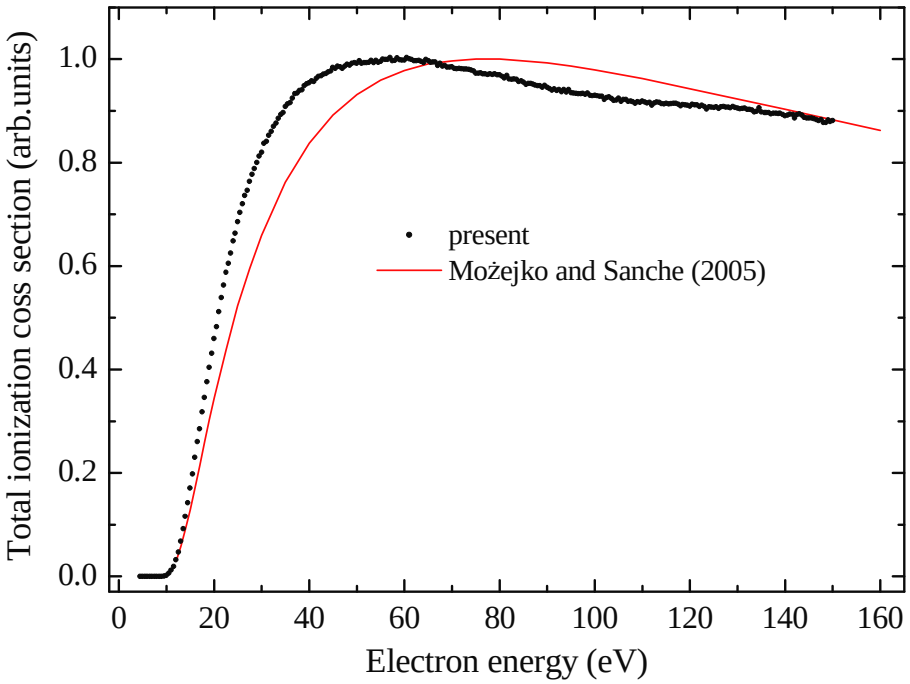
Total ionization coss section (arb.units)
Electron energy (eV)
present
Możejko and Sanche (2005)

Fig. 5